

Tensor-network study of the ground state of maple-leaf Heisenberg antiferromagnet

Samuel Nyckees,^{1,2} Pratyay Ghosh,^{1,*} and Frédéric Mila¹

¹*Institute of Physics, Ecole Polytechnique Fédérale de Lausanne (EPFL), CH-1015 Lausanne, Switzerland*

²*Now at Université Grenoble Alpes, CEA List, 38000 Grenoble, France*

We study the quantum phase diagram of the spin-1/2 nearest-neighbor Heisenberg model on the maple-leaf lattice using infinite projected entangled pair states (iPEPS) combined with a corner transfer matrix renormalization group scheme adapted to C_3 -symmetric lattices. Focusing on the fully antiferromagnetic J - J_d model with $J_h = J_t := J$, we map out the ground-state phase diagram as a function of the dimer coupling J_d . Our results show that the system hosts only two phases: a magnetically ordered canted-120° phase and an exact dimer singlet product phase. We identify a first-order transition between these two phases at $J_d/J \approx 1.45$. Within the magnetically ordered phase, we observe small but finite magnetic moments. We also resolve the quantum renormalization of the canting angle, which deviates from the classical prediction over almost the entire magnetically ordered phase.

I. INTRODUCTION

Quantum antiferromagnets on frustrated lattices are prototypical systems in which competing interactions or lattice geometry prevent spins from simultaneously satisfying all constraints, often resulting in highly degenerate ground states and unconventional magnetic or exotic quantum-disordered phases [1, 2]. Against this backdrop, the $S = 1/2$ Heisenberg antiferromagnet on the maple-leaf lattice (MLL) [3] has recently become an active topic of investigations due to its ability to host an exact dimer product ground state [4, 5], spin liquid phases [6–8], unusual canted magnetic order [4, 5, 9], and predicted exotic magnetization plateaus formed by multi-particle bound states [10]. Moreover, several material realizations exist in which the underlying lattice of magnetic ions follow the maple-leaf structure [11–16], further enhancing interest in the magnetic properties of this system.

The MLL [see Fig. 1(a)] is one of the eleven Archimedean lattices and has a coordination number of five. It can be viewed as one-seventh site-depleted (one-fifth bond-depleted) triangular lattice [4, 18, 19]. The lattice contains three symmetry-inequivalent nearest-neighbor bonds, which can be assigned three different interaction strengths: J_h on the hexagons, J_t on the triangles, and J_d on the dimers, as shown in Fig. 1(a). The spin-1/2 Heisenberg model on the MLL is thus given by

$$H = \sum_{\langle ij \rangle_k} J_k \mathbf{S}_i \cdot \mathbf{S}_j, \quad (1)$$

where \mathbf{S}_i are spin-1/2 operators and $\langle ij \rangle_k$ denotes a nearest-neighbor bond of type $k \in \{h, t, d\}$. A central focus of theoretical investigations of the fully antiferromagnetic model on the MLL is the case $J_h = J_t := J$, with the phase diagram explored as a function of J_d . The earliest study of this model was carried out by Richter *et al.* using the coupled cluster method (CCM) and exact diagonalization [4]. Their results suggest that the

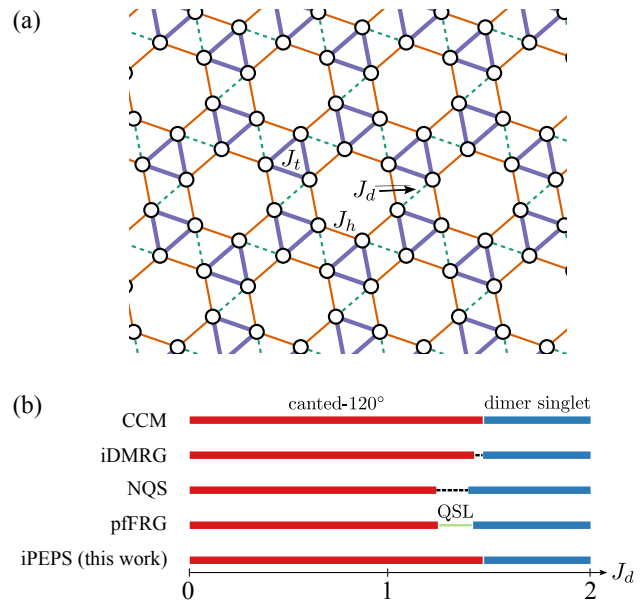


FIG. 1. (a) Maple-leaf lattice (MLL) with nearest-neighbor interactions. The green dashed bonds denote the dimer couplings J_d , while the thick violet and thin red bonds represent the inter-dimer couplings J_t and J_h , respectively. (b) Ground-state phase diagram of the Heisenberg model on the maple-leaf lattice with $J_h = J_t = 1$ as a function of J_d , obtained using different numerical techniques, including the present work. Both CCM [4] and our iPEPS simulations find that the system realizes only two phases, namely the canted-120° ordered phase and the product dimer singlet phase, separated by a first-order transition at $J_d \approx 1.45$. The iDMRG [17] and NQS calculations [17] also identify these two phases, but with an intervening region of uncertainty between them, indicated by the dashed lines. In contrast, the pseudofermion functional renormalization group study [6] reports a quantum spin liquid phase between the canted-120° ordered phase and the product dimer singlet phase.

phase diagram hosts only two phases, namely an unusual magnetically ordered phase, identified as canted-120° order, and an exact dimer singlet product phase. The phase transition between these two phases was found to

* pratyay.ghosh@epfl.ch

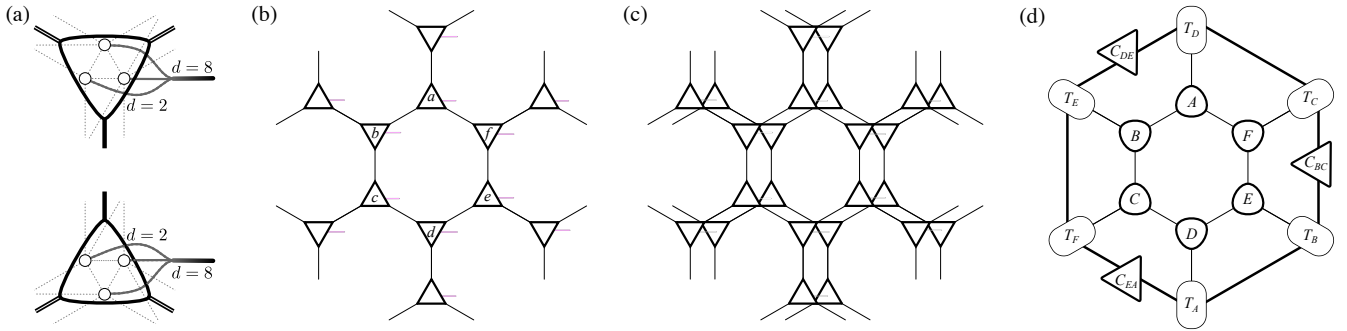


FIG. 2. (a) Coarse-grained three-site tensors. Each J_t trimer of the lattice is represented by a tensor with physical dimension $d = 8$. The thick black lines indicate virtual bonds of dimension D . (b) Two-dimensional iPEPS wave function defined on a honeycomb network with a six-site unit cell. The gray lines denote the physical legs. (c) The wave-function overlap is represented by the contraction of an infinite tensor network. (d) This contraction is approximated by an effective environment composed of row and corner tensors. The thicker black lines indicate environment bonds of dimension χ .

occur at $J_d/J \approx 1.45$ [4]. Subsequent studies employing pseudofermion functional renormalization group (pF-FRG) [6], infinite-density matrix renormalization group (iDMRG) [17], and neural quantum states (NQS) [17] are largely consistent with these findings. These studies, however, also raise the possibility of an intermediate phase located between the canted-120° ordered phase and the exact dimer phase; the iDMRG identify an intervening valence bond-like phase whose true nature remains unresolved, whereas the pF-FRG approach reports a quantum spin liquid (QSL) ground phase. A comprehensive overview of the phase diagrams obtained from different numerical techniques (together with the results of the present work) is shown in Fig. 1(b).

In this article, we examine the spin-1/2 nearest-neighbor antiferromagnetic Heisenberg model on the MLL. We set $J = 1$ throughout this work and investigate the system as a function of J_d using the state-of-the-art tensor network method of infinite projected entangled pair states (iPEPS), together with a specialized corner transfer matrix renormalization group scheme adapted to C_3 -symmetric systems to approximate the environment [20–25]. iPEPS is a variational ansatz in which the wave function of a two-dimensional infinite system is represented through a network of tensors [26–30], allowing direct access to the ground state properties in the thermodynamic limit. Our iPEPS simulations show that the ground-state phase diagram contains only the canted-120° ordered phase and the exact dimer singlet phase, in agreement with the findings of CCM [4], with no evidence for an intermediate phase. We find a first-order phase transition between these two phases at $J_d \approx 1.45$.

The remainder of the article is organized as follows. In Sec. II, we describe the iPEPS methodology used to study the maple-leaf Heisenberg antiferromagnet. In Sec. III, we present the ground-state phase diagram of the model. Finally, Sec. IV summarizes our main findings and outlines directions for future research.

II. INFINITE PROJECTED ENTANGLED PAIR STATES (IPEPS)

The iPEPS ansatz represents the ground-state wave function of a two-dimensional system as an infinite two-dimensional tensor network. In this work, we consider a tensor network in which each J_t trimer of the MLL is represented by a single tensor with a physical leg of dimension $d = 2^3$ [Fig. 2(a)]. This construction leads to a representation of the ground state as a tensor network defined on the honeycomb lattice, with tensors $a_{i,j,k,s}^{[\mathbf{x}]}$ [see Fig. 2(b)], where the indices i, j, k label the virtual spaces of dimension D , and the index s corresponds to the physical space. The position of each tensor within the unit cell is denoted by $[\mathbf{x}]$.

To obtain the ground state, the tensors $a_{i,j,k,s}^{[\mathbf{x}]}$ are optimized by minimizing the energy of the system. Various optimization strategies exist, including the simple update [26], full update [27, 32], and automatic differentiation [33]. In this work, we employ the simple update algorithm, in which a random initial tensor network $|\psi_0\rangle$ is evolved in imaginary time through a sequence of local, quasi-adiabatic updates, mimicking a slow annealing process that relaxes the system toward the ground state $|\psi\rangle$. For gapped systems, where entanglement is relatively short-ranged, this approach provides an efficient and accurate approximation of the ground state. The imaginary-time evolution is implemented by iteratively applying a Trotter–Suzuki decomposition of $e^{-\tau H}$,

$$|\psi\rangle = \lim_{\beta \rightarrow \infty} e^{-\beta H} |\psi_0\rangle \quad (2)$$

$$\simeq \lim_{n \rightarrow \infty} \left(\prod_{e \in \langle i,j \rangle} e^{-\tau H_e} \right)^n |\psi_0\rangle. \quad (3)$$

In practice, we use $\tau = 10^{-3}$ – 10^{-2} . The imaginary-time evolution is carried out using two-site gates that are successively applied to nearest-neighbor tensors. After each gate application, the local tensors $a^{[\mathbf{x}]}$ are projected back

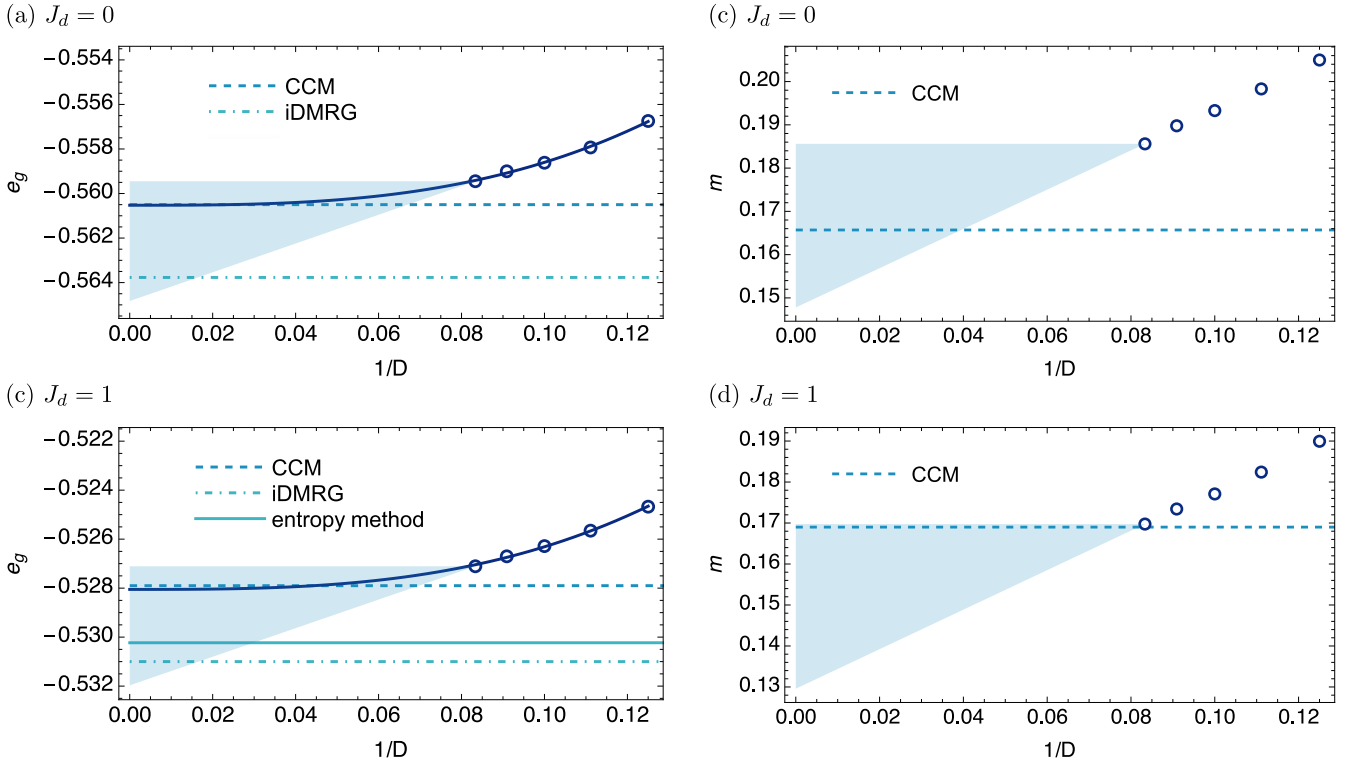


FIG. 3. Scaling of the ground-state energy per site, e_g , obtained from iPEPS as a function of $1/D$ at $J_h = J_t = 1$ for (a) $J_d = 0$ and (b) $J_d = 1$. Energies obtained using different numerical approaches, namely CCM [4], iDMRG [17], and entropy method [31], are also indicated. The dark solid lines show the $D \rightarrow \infty$ extrapolations obtained by fitting the data. The shaded regions represent estimates of the error bars, where the upper bounds correspond to the energies at $D = 12$, and the lower bounds are obtained from a linear extrapolation of the $D = 11$ and $D = 12$ data. Scaling of the average local magnetic moment, m , obtained from iPEPS as a function of $1/D$ at $J_h = J_t = 1$ for (c) $J_d = 0$ and (d) $J_d = 1$. Conservative error bar estimates for m , indicated by the shaded regions, are obtained in the same manner as for the energy.

onto a relevant subspace of dimension D by performing a singular value decomposition and retaining only the D largest singular values.

Once the local tensors have been optimized, local observables are evaluated by contracting the infinite two-dimensional tensor network defined in terms of the local tensor

$$A_{i,i',j,j',k,k'}^{[\mathbf{x}]} = a_{i',j',k',s}^{[\mathbf{x}]\dagger} a_{i,j,k,s}^{[\mathbf{x}]}$$

see Fig. 2(c). To perform this contraction, we employ the corner transfer matrix renormalization group (CTMRG) algorithm specifically designed for tensor networks on the honeycomb lattice [20–25]. The CTMRG approximates the infinite contraction using an effective environment composed of row tensors $T^{[\mathbf{x}]}$ and corner tensors $C^{[\mathbf{x}]}$, as illustrated in Fig. 2(d), with dimensions $\chi \times D^2 \times \chi$ and $\chi \times \chi$, respectively. The parameter χ serves as a control parameter, and one expects the contraction to converge to the exact result in the limit $\chi \rightarrow \infty$. In practice, it is necessary to verify that observables, such as the energy, are converged with respect to χ . In this study, we use χ up to 120, for which the energy has sufficiently converged (with a precision of 10^{-6}) for all bond dimensions $D \in [8, 12]$.

III. GROUND STATE PHASE DIAGRAM

We begin by discussing two special points of (1), namely $J_d = 0$ and $J_d = 1$. In the first case, the Hamiltonian reduces to the uniform antiferromagnetic Heisenberg model on the ruby lattice (also known as the bounce lattice). This limit has been studied in several works as part of the phase diagram of the MLL [4, 6, 17], all of which report a magnetically ordered ground state. However, Ref. [34] finds a valence bond crystal ground state via iPEPS simulations, with a ground-state energy of -0.545089 per site at $D = 12$. In our iPEPS calculations, we obtain a ground-state energy of -0.559448 , which is significantly lower than the previous iPEPS estimate, at the same bond dimension [see Fig. 3(a)]. This result is in excellent agreement with the results obtained from CCM and other numerical methods. In Fig. 3(c), we show the variation of the average local magnetic moment,

$$m = \frac{1}{6} \sum_{i=1}^6 |\langle \vec{S}_i \rangle|,$$

where i runs over the magnetic unit cell, as a function of $1/D$. The data indicates a finite m as $D \rightarrow \infty$.

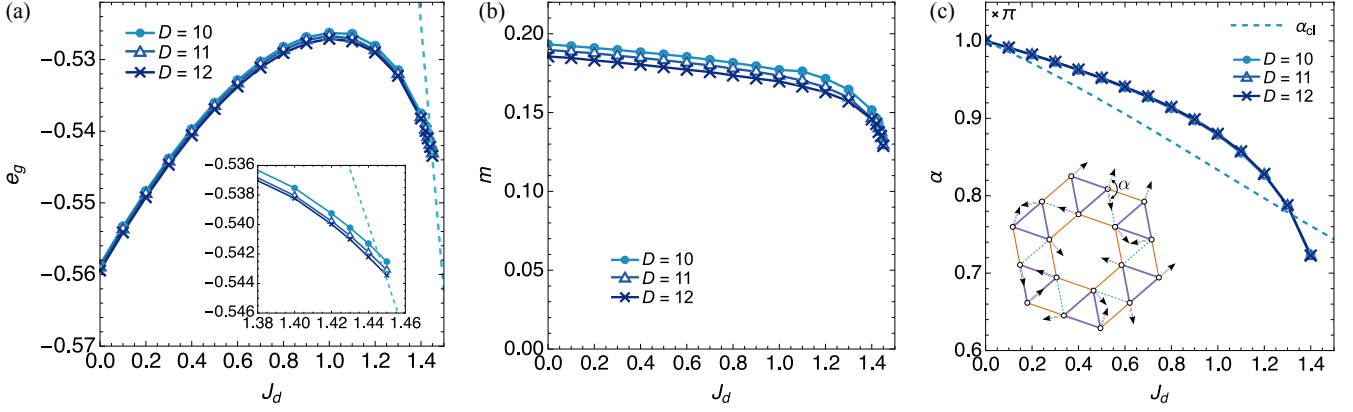


FIG. 4. (a) Energy of the canted-120° ordered ground state as a function of J_d , obtained from iPEPS calculations for different bond dimensions D . The dashed line indicates the energy of the exact dimer singlet product state. The transition between the canted-120° phase and the exact dimer phase is clearly first order, as can be seen in the inset. (b) Dependence of the local spin moment, m , in the canted-120° phase on J_d , obtained from iPEPS calculations for various bond dimensions D . (c) Canting angle α as a function of J_d . The definition of the canting angle is shown in the inset. The dashed curve corresponds to the classical canting angle α_{cl} [see Eq. (4)].

The $J_d = 1$ limit has been studied using several numerical approaches [4, 6, 17, 19, 31], all of which report magnetic ordering. Our iPEPS calculations confirm this behavior. In Fig. 3(b), we show the ground-state energy as a function of $1/D$, compared with results from other numerical methods. In Fig. 3(d), we display the corresponding dependence of m on D , indicating magnetic ordering in the $D \rightarrow \infty$ limit.

The spin moments obtained in our calculations for both $J_d = 0$ and $J_d = 1$ are small and comparable to the orderer magnetic moment found in the spin-1/2 nearest-neighbor Heisenberg model on the triangular lattice [35]. In the ideal maple-leaf limit, the magnetic moment is $m = 0.1697$ (at $D = 12$), while for the ruby lattice the moment is slightly larger, $m = 0.1856$. The local magnetizations and ground-state energies at both limits are summarized in Table I, together with a comparison to results obtained using other numerical techniques. The numbers corresponding to m in Table I should be considered as upper bounds, since they decrease systematically with decreasing $1/D$. However, even under conservative linear extrapolations, which likely provide lower bounds, the magnetic moment remains non-negligible.

We now turn to the remaining parts of the phase diagram. It can be shown analytically that the ground state of the Heisenberg model for $J_d \geq 2$ is an exact product state of singlets on the dimer bonds [5]. This analysis, however, is based on a variational argument and does not preclude the system from realizing the same product singlet state for $J_d < 2$. Our iPEPS calculations show that this state ceases to be the ground state at $J_d \approx 1.45$. For $J_d \lesssim 1.44$, the system develops a magnetic order, which persists down to $J_d = 0$. In Fig. 4(a), we show the evolution of the ground-state energy per site as a function of J_d . To pinpoint the phase transition, we continue to evaluate the energy of the canted-120° state

	$J_d = 0$	$J_d = 1$
e_g		
CCM [4]	-0.5605	-0.5279
NQS [17]	-0.549897	-0.523571
iDMRG [17]	-0.56376	-0.53100
Entropy method [31]	-	-0.5304(2)
iPEPS [34]	-0.545089	-
iPEPS	-0.560526	-0.528052
m		
CCM [4]	0.1657	0.1690
NQS [17]	0.151673	-
iPEPS ($D = 12$)	0.1856	0.1697

TABLE I. Comparison of ground state energy per site (e_g) and average local magnetic moment (m) obtained from our iPEPS simulations with other numerical approaches. The iPEPS results obtained in the present work are highlighted in bold. The values of m correspond to $D = 12$ and therefore provide upper bounds for the local magnetizations.

even beyond its stability region, allowing a direct comparison with the energy of the dimer singlet state in the vicinity of the transition. This allows us to identify a first-order transition between the two phases occurring within $1.44 < J_d < 1.45$ [see the inset of Fig. 4(a)] and to rule out the presence of any intermediate phase.

We also compute the average local magnetic moment m throughout the magnetically ordered phase using iPEPS simulations. In Fig. 4(b), we show the behavior of m as a function of J_d for different bond dimensions D . The magnetic moment exhibits only a weak dependence on J_d . In this phase, the system adopts the classical canted-120° order shown in Fig. 4(c) [5, 6, 13, 17], which can be understood as a local 120° order on individual J_t triangles, with a relative canting of the magnetic moments between neighboring triangles. This type of magnetic order is unique to the MLL. The canting is determined by the

competition between the J_h and J_d bonds and is therefore expected to vary with J_d . One way to parametrize this canting is via the relative angle α between the spin moments across the J_h bonds [see Fig. 4 (c)]. In the classical $S \rightarrow \infty$ limit, α can be obtained from a Luttinger-Tisza analysis [5, 36] as

$$\alpha_{\text{cl}} = \pi - \arccos \left(\frac{4 - J_d}{2\sqrt{J_d^2 - 2J_d + 4}} \right). \quad (4)$$

Quantum fluctuations are expected to renormalize this angle. To determine α , we compute the components of the local spin moments on the sites within a single unit cell and extract the relative angles between moments across the J_h bonds. In Fig. 4(c), we present the canting angle α as a function of J_d obtained from our iPEPS calculations. We find that α deviates significantly from the classical prediction over most of the magnetically ordered phase, except at $J_d = 0$, where it coincides with α_{cl} . The canting angles obtained from iPEPS are in excellent agreement with CCM results [4].

IV. CONCLUSIONS AND DISCUSSIONS

We have explored the quantum phase diagram of the nearest-neighbor antiferromagnetic Heisenberg model on the maple-leaf lattice (MLL) using the iPEPS approach combined with a CTMRG scheme suited for C_3 -symmetric lattices. Our study focuses on the J - J_d model on the MLL, for which one expects an exact dimer singlet product ground state to emerge for sufficiently large J_d . We find that the exact dimer state stabilizes for $J_d/J \gtrsim 1.45$. Below this ratio, the system exhibits a canted-120° magnetically ordered phase with a small magnetic moment. We identify a first-order phase transition between these two phases. Moreover, we could resolve the spin canting between neighboring trimer motifs within the magnetically ordered phase. Our results are in agreement with previously reported numerical stud-

ies. We also emphasize that our simulations can capture ground states with unit cells of up to eighteen sites. Within this framework, we find no evidence for an additional intermediate phase, as reported in Ref. [6] or suggested in Ref. [17]. We would further like to note that the CCM developed by Richter and coworkers [37, 38] provides a highly reliable and internally consistent description of the MLL antiferromagnet, and more generally of quantum spin systems with magnetically ordered phases, yielding quantitatively accurate energies and order parameters that serve as a valuable benchmark for modern numerical approaches [39].

There are two recent preprints [8, 40] that also study the same model and report ground states that differ from ours, and, by extension, from earlier studies. The former employs iPEPS simulations with an automatic-differentiation-based optimization scheme and finds that the canted-120° order stabilizes only in a narrow region adjacent to the exact dimer phase. The remainder of the phase diagram down to $J_d = 0$ is reported to be magnetically disordered. The authors further claim that the ground state at $J_d = 0$ is a gapless spin liquid, while the state at $J_d = 1$ is a gapped spin liquid. The latter work [40] uses numerical linked-cluster expansions to study the model at $J_d = 1$ and finds a short-range correlated paramagnetic ground state composed of resonating hexagonal motifs. The energies obtained in these studies differ only marginally from those found in our simulations. These results suggest that the model hosts several closely competing low-energy states, reflecting the subtle selection of its ground state. Exploring the system along alternative parametric trajectories [7, 9, 41] or under different perturbations could uncover the underlying complexity of the MLL phase diagram.

Acknowledgments: This work is dedicated to the memory of Johannes Richter. The work at EPFL was supported by the Swiss National Science Foundation under Grant No. 212082. Numerical computations were performed using the facilities of the Scientific IT and Application Support Center of EPFL (SCITAS).

The iPEPS data are openly available [42].

[1] C. Lacroix, P. Mendels, and F. Mila, *Introduction to Frustrated Magnetism: Materials, Experiments, Theory*, Springer Series in Solid-State Sciences (Springer Berlin Heidelberg, 2011).

[2] H. T. Diep, *Frustrated Spin Systems* (WORLD SCIENTIFIC, 2012).

[3] D. D. Betts, A new two-dimensional lattice of coordination number five, *Proc. N. S. Inst. Sci.* **40**, 95 (1995).

[4] D. J. J. Farnell, R. Darradi, R. Schmidt, and J. Richter, Spin-half heisenberg antiferromagnet on two archimedean lattices: From the bounce lattice to the maple-leaf lattice and beyond, *Phys. Rev. B* **84**, 104406 (2011).

[5] P. Ghosh, T. Müller, and R. Thomale, Another exact ground state of a two-dimensional quantum antiferromagnet, *Phys. Rev. B* **105**, L180412 (2022).

[6] L. Gresista, C. Hickey, S. Trebst, and Y. Iqbal, Candidate quantum disordered intermediate phase in the heisenberg antiferromagnet on the maple-leaf lattice, *Phys. Rev. B* **108**, L241116 (2023).

[7] P. Ghosh, Triplon analysis of magnetic disorder and order in maple-leaf heisenberg magnet, *J. Phys. Condens. Matter* **36**, 455803 (2024).

[8] P. Schmoll, J. Naumann, J. Eisert, and Y. Iqbal, Bathing in a sea of candidate quantum spin liquids: From the gapless ruby to the gapped maple-leaf lattice (2024), arXiv:2407.07145 [cond-mat.str-el].

[9] M. Gembé, L. Gresista, H.-J. Schmidt, C. Hickey, Y. Iqbal, and S. Trebst, Noncoplanar orders and quantum disordered states in maple-leaf antiferromagnets, *Phys. Rev. B* **110**, 085151 (2024).

[10] P. Ghosh, J. Seufert, T. Müller, F. Mila, and R. Thomale, Maple leaf antiferromagnet in a magnetic field, *Phys. Rev. B* **108**, L060406 (2023).

[11] Y. Haraguchi, A. Matsuo, K. Kindo, and Z. Hiroi, Quantum antiferromagnet bluebellite comprising a maple-leaf lattice made of spin-1/2 Cu^{2+} ions, *Phys. Rev. B* **104**, 174439 (2021).

[12] C. Aguilar-Maldonado, R. Feyerherm, K. Prokeš, L. Keller, and B. Lake, Structure and magnetic properties of the maple leaf antiferromagnet ho_3sc_6 , *Phys. Rev. B* **111**, 094439 (2025).

[13] T. Fennell, J. O. Piatek, R. A. Stephenson, G. J. Nilsen, and H. M. Rønnow, Spangolite: ans= 1/2 maple leaf lattice antiferromagnet?, *J. Phys.: Condens. Matter* **23**, 164201 (2011).

[14] P. Schmoll, H. O. Jeschke, and Y. Iqbal, Tensor network analysis of the maple-leaf antiferromagnet spangolite, *Communications Materials* **6**, 10.1038/s43246-025-00904-1 (2025).

[15] P. Ghosh, T. Müller, Y. Iqbal, R. Thomale, and H. O. Jeschke, Effective spin-1 breathing kagome hamiltonian induced by the exchange hierarchy in the maple leaf mineral bluebellite, *Phys. Rev. B* **110**, 094406 (2024).

[16] P. Ghosh, Chiral crossroads in ho_3sc_6 : Competing interactions on the maple-leaf lattice, *Phys. Rev. B* **111**, 224431 (2025).

[17] J. Beck, J. Bodky, J. Motruk, T. Müller, R. Thomale, and P. Ghosh, Phase diagram of the $J-J_d$ heisenberg model on the maple leaf lattice: Neural networks and density matrix renormalization group, *Phys. Rev. B* **109**, 184422 (2024).

[18] J. Schulenburg, J. Richter, and D. Betts, Heisenberg antiferromagnet on a 1/7-depleted triangular lattice, *Acta Physica Polonica-Series A General Physics* **97**, 971 (2000).

[19] D. Schmalfuß, P. Tomczak, J. Schulenburg, and J. Richter, The spin- $\frac{1}{2}$ heisenberg antiferromagnet on a $\frac{1}{7}$ -depleted triangular lattice: Ground-state properties, *Phys. Rev. B* **65**, 224405 (2002).

[20] A. Gendiar, R. Krcmar, S. Andergassen, M. Daniška, and T. Nishino, Weak correlation effects in the ising model on triangular-tiled hyperbolic lattices, *Phys. Rev. E* **86**, 021105 (2012).

[21] S. Nyckees, A. Rufino, F. Mila, and J. Colbois, Critical line of the triangular ising antiferromagnet in a field from a C_3 -symmetric corner transfer matrix algorithm, *Phys. Rev. E* **108**, 064132 (2023).

[22] I. V. Lukin and A. G. Sotnikov, Variational optimization of tensor-network states with the honeycomb-lattice corner transfer matrix, *Phys. Rev. B* **107**, 054424 (2023).

[23] I. V. Lukin and A. G. Sotnikov, Corner transfer matrix renormalization group approach in the zoo of archimedean lattices, *Phys. Rev. E* **109**, 045305 (2024).

[24] P. Ghosh, J. A. Koziol, S. Nyckees, K. P. Schmidt, and F. Mila, Symmetry breaking and competing valence bond states in the star lattice heisenberg antiferromagnet, *Phys. Rev. B* **112**, 144423 (2025).

[25] P. Ghosh and F. Mila, Simplex crystal ground state and magnetization plateaus in the spin-1/2 heisenberg model on the ruby lattice (2025), arXiv:2512.14173 [cond-mat.str-el].

[26] H. C. Jiang, Z. Y. Weng, and T. Xiang, Accurate determination of tensor network state of quantum lattice models in two dimensions, *Phys. Rev. Lett.* **101**, 090603 (2008).

[27] J. Jordan, R. Orús, G. Vidal, F. Verstraete, and J. I. Cirac, Classical simulation of infinite-size quantum lattice systems in two spatial dimensions, *Phys. Rev. Lett.* **101**, 250602 (2008).

[28] F. Verstraete and J. I. Cirac, Valence-bond states for quantum computation, *Phys. Rev. A* **70**, 060302 (2004).

[29] F. Verstraete and J. I. Cirac, Renormalization algorithms for quantum-many body systems in two and higher dimensions (2004), arXiv:cond-mat/0407066 [cond-mat.str-el].

[30] Z.-C. Gu, M. Levin, and X.-G. Wen, Tensor-entanglement renormalization group approach as a unified method for symmetry breaking and topological phase transitions, *Phys. Rev. B* **78**, 205116 (2008).

[31] T. Hutak, Thermodynamics of the $s = \frac{1}{2}$ maple-leaf heisenberg antiferromagnet, *Phys. Rev. B* **112**, 104405 (2025).

[32] H. N. Phien, J. A. Bengua, H. D. Tuan, P. Corboz, and R. Orús, Infinite projected entangled pair states algorithm improved: Fast full update and gauge fixing, *Physical Review B* **92**, 10.1103/physrevb.92.035142 (2015).

[33] J. Hasik, D. Poilblanc, and F. Becca, Investigation of the Néel phase of the frustrated Heisenberg antiferromagnet by differentiable symmetric tensor networks, *SciPost Phys.* **10**, 012 (2021).

[34] S. S. Jahromi and R. Orús, Topological F_2 resonating-valence-bond quantum spin liquid on the ruby lattice, *Phys. Rev. B* **101**, 115114 (2020).

[35] J. Hasik and P. Corboz, Incommensurate order with translationally invariant projected entangled-pair states: Spiral states and quantum spin liquid on the anisotropic triangular lattice, *Phys. Rev. Lett.* **133**, 176502 (2024).

[36] J. M. Luttinger and L. Tisza, Theory of dipole interaction in crystals, *Phys. Rev.* **70**, 954 (1946).

[37] R. F. Bishop, D. J. J. Farnell, S. E. Krüger, J. B. Parkinson, J. Richter, and C. Zeng, High-order coupled cluster method calculations for the ground- and excited-state properties of the spin-halfxxzmodel, *Journal of Physics: Condensed Matter* **12**, 6887–6902 (2000).

[38] J. Richter, R. Darradi, R. Zinke, and R. Bishop, Frustrated quantum antiferromagnets: Application of high-order coupled cluster method, *International Journal of Modern Physics B* **21**, 2273 (2007).

[39] J. Naumann, E. L. Weerda, M. Rizzi, J. Eisert, and P. Schmoll, An introduction to infinite projected entangled-pair state methods for variational ground state simulations using automatic differentiation, *SciPost Phys. Lect. Notes* , 86 (2024).

[40] R. Schäfer, P. L. Ebert, N. Hassan, J. Reuther, D. J. Luitz, and A. Wietek, Thermodynamics of the heisenberg antiferromagnet on the maple-leaf lattice (2025), arXiv:2511.21806 [cond-mat.str-el].

[41] P. Ghosh and B. Kumar, Spontaneous dimerization and moment formation in the Hida model of the spin-1 kagome antiferromagnet, *Phys. Rev. B* **97**, 014413 (2018).

[42] P. Ghosh, F. Mila, and S. Nyckees, Maple-leaf ipps (2025).